Title

Supramolecular Porphyrin Cages Assembled at Molecular–Materials Interfaces for Electrocatalytic CO Reduction

Journal

ACS Central Science, 3(9)

ISSN

2374-7943

Authors

Gong, Ming
Cao, Zhi
Liu, Wei
et al.

Publication Date

2017-09-27

DOI

10.1021/acscentsci.7b00316

Peer reviewed

ACS central science

Research Article

http://pubs.acs.org/journal/acscii

Supramolecular Porphyrin Cages Assembled at Molecular−Materials Interfaces for Electrocatalytic CO Reduction

Ming Gong,[†,‡,§] Zhi Cao,[†,§] Wei Liu,[†,§,∥] Eva M. Nichols,[†,‡] Peter T. Smith,[†] Jeffrey S. Derrick,[†,‡] Yi-Sheng Liu,[⊥] Jinjia Liu,[#] Xiaodong Wen,[#,Δ] and Christopher J. Chang*[,†,‡,∥,¶]

[†]Department of Chemistry, [¶]Department of Molecular and Cell Biology, and [∥]Howard Hughes Medical Institute, University of California, Berkeley, California 94720, United States

[‡]Chemical Sciences Division and [⊥]The Advanced Light Source, Lawrence Berkeley National Laboratory, Berkeley, California 94720, United States

[#]Institute of Coal Chemistry, Chinese Academy of Sciences, Taiyuan, Shanxi 030001, China

[Δ]Synfuels China, Beijing, 100195, China

Supporting Information

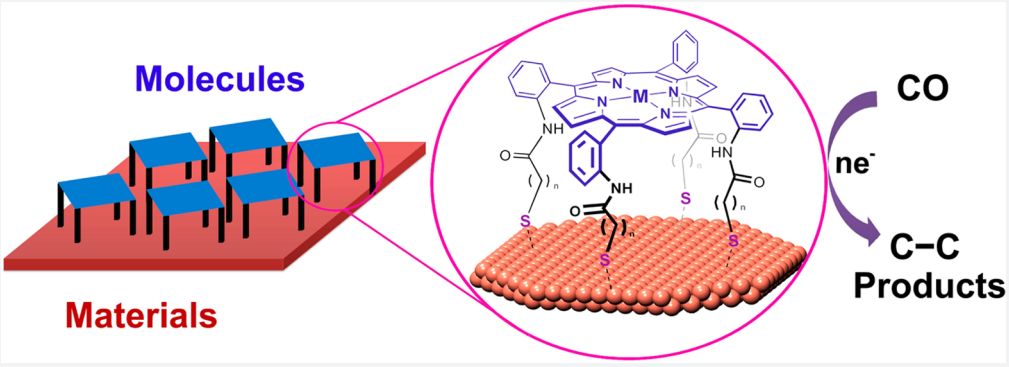

ABSTRACT: Conversion of carbon monoxide (CO), a major one-carbon product of carbon dioxide (CO_2) reduction, into value-added multicarbon species is a challenge to addressing global energy demands and climate change. Here we report a modular synthetic approach for aqueous electrochemical CO reduction to carbon−carbon coupled products via self-assembly of supramolecular cages at molecular−materials interfaces. Heterobimetallic cavities formed by face-to-face coordination of thiol-terminated metalloporphyrins to copper electrodes through varying organic struts convert CO to C2 products with high faradaic efficiency (FE = 83% total with 57% to ethanol) and current density (1.34 mA/cm^2) at a potential of −0.40 V vs RHE. The cage-functionalized electrodes offer an order of magnitude improvement in both selectivity and activity for electrocatalytic carbon fixation compared to parent copper surfaces or copper functionalized with porphyrins in an edge-on orientation.

INTRODUCTION

Climate change and rising global energy demands motivate broad interest in carbon fixation to value-added products with formation of carbon−carbon bonds.[1−6] In this context, carbon monoxide (CO) is a common one-carbon product of carbon dioxide (CO_2) reduction[7−27] and major feedstock for producing multicarbon products as illustrated by the classic Fischer−Tropsch process.[28,29] Electrochemical CO reduction offers a complementary approach to C−C coupling reactivity with sustainable energy input,[30−33] where reducing hydrogen equivalents can be provided directly by aqueous electrolytes and thus bypass the traditionally energy-intensive steam reforming process for H_2 production. Reports of electrochemical CO reduction are exceedingly rare relative to CO_2 reduction and have focused largely on copper, which can reduce CO to C2 products including ethanol, acetate, and ethylene; however, conventional Cu electrodes show poor selectivity for CO over proton reduction and low energetic efficiency.[33] Elegant work by Kanan et al. has utilized grain boundaries to improve CO over H^+ selectivity on nanocrystalline Cu materials,[30−32] but optimizing CO electroreduction catalysts at a molecular level to attain both high specificity and activity remains a significant challenge. In this regard, Nature provides inspiration for CO catalysis in the form of CO dehydrogenase enzymes (CODHs),[34−38] which drive efficient CO catalysis through self-assembly of heterobimetallic cavities (e.g., NiFe or MoCu) with pendant electron reservoirs.

Against this backdrop, we sought to synthesize electrocatalysts for CO reduction that could combine these key bioinorganic features yet allow for molecular-level tunability. We now report a supramolecular approach to CO electro-

Received: July 16, 2017
Published: September 13, 2017

DOI: 10.1021/acscentsci.7b00316
ACS Cent. Sci. 2017, 3, 1032−1040

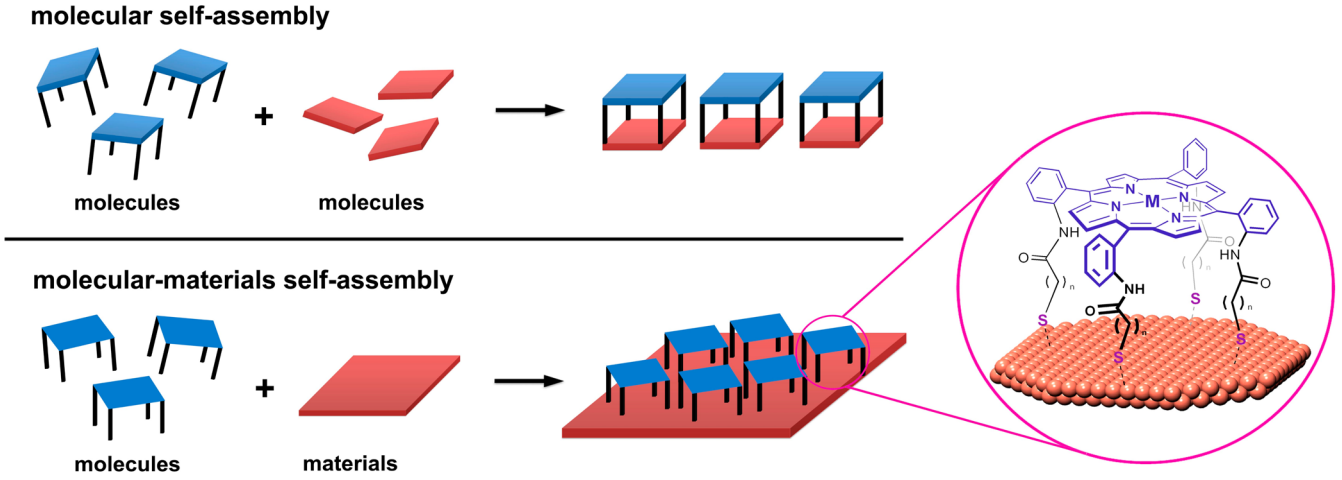

Figure 1. Schematic illustration of traditional supramolecular assembly of cages between molecular components and supramolecular assembly of cages between molecular and materials components, as illustrated by formation of porphyrin cages on electrode surfaces.

Scheme 1. A. Synthetic Procedures for the Preparation of Thiolate-Containing Porphyrins.[a] B. Structures of Porphyrins Used in This Study

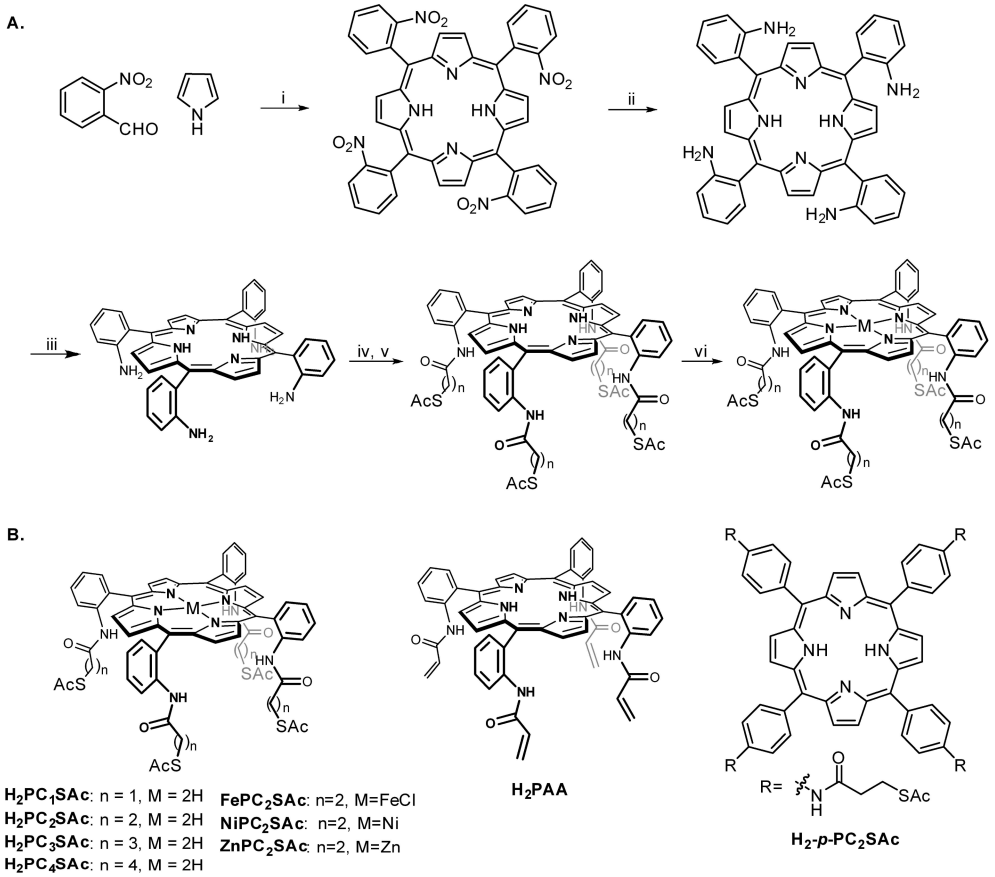

[a](i) Acetic acid, reflux, 1 h; (ii) $SnCl_2$, 12 N HCl, 65°C; (iii) silica gel, benzene, 80 °C, 20 h; (iv) n = 1, bromoacetyl bromide; n = 2, 3-bromopropionyl bromide; n = 3, 4-chlorobutyryl chloride; n = 4, 5-chlorovaleroyl chloride; (v) KSAc, THF, 4 h; (vi) MCl_2 (M= Fe, Zn, and Ni), 2,6-lutidine, THF.

catalysis in which heterobimetallic cages can be assembled directly at molecular−materials interfaces from systematically tunable building blocks. Specifically, we show that metalloporphyrins bearing thiol-terminated organic struts form synthetic cavities of predictable sizes and metal−metal distances upon cofacial interactions with Cu electrodes, enabling electrochemical CO reduction with high selectivity and activity for C2 products (Figure 1). In addition to introducing interfacial supramolecular chemistry as a versatile design principle for an important catalytic carbon fixation process, this work provides a starting point for merging molecular and materials catalyst components through supramolecular self-

DOI: 10.1021/acscentsci.7b00316
ACS Cent. Sci. 2017, 3, 1032−1040

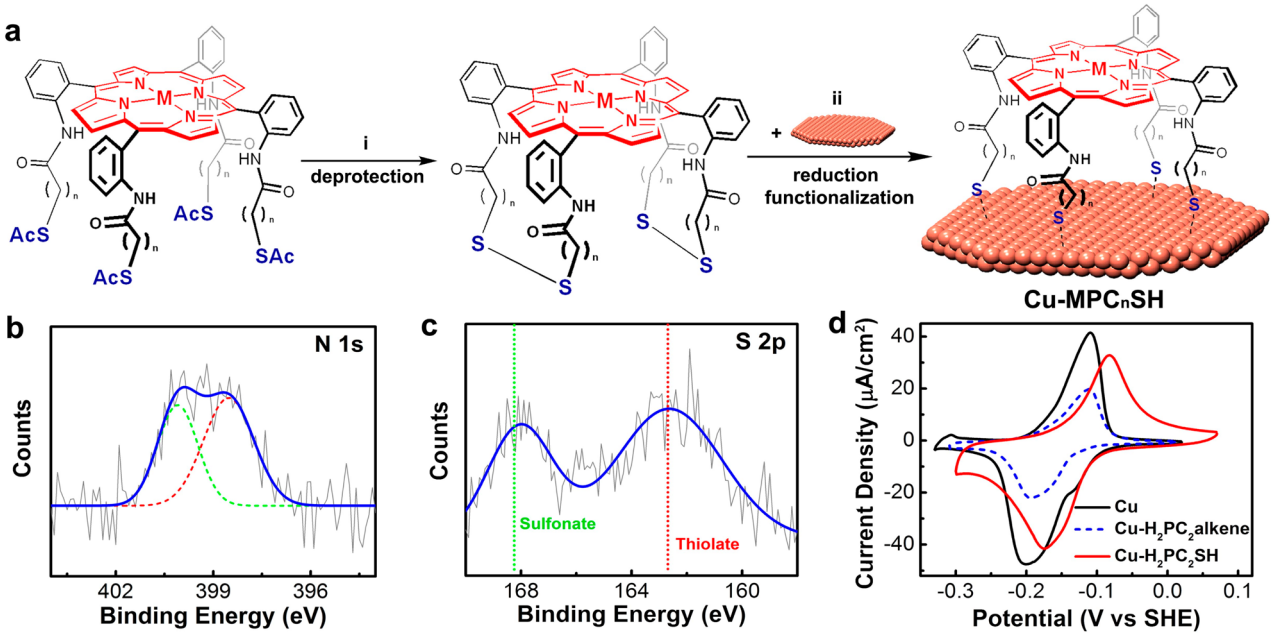

Figure 2. (a) Schematic illustration of the functionalization of Cu surfaces with porphyrin cages. (i) NH_3 in methanol/chloroform, 25 °C, 4 h; (ii) sodium borohydride, DMF, 25 °C, 12 h. (b) High resolution N 1s and (c) S 2p XPS spectra of 100 nm Cu on Si wafer functionalized with porphyrin cages. (d) Cyclic voltammetry curves of underpotential deposition of Pb on Cu (black), Cu tethered with alkene-terminated porphyrins (dashed blue), and Cu tethered with thiol-terminated porphyrins (red). The scan rate is 10 mV/s.

assembly for a broader range of chemical transformations and applications.

RESULTS AND DISCUSSION

Design, Synthesis, and Characterization of Porphyrin Caps for Formation of Supramolecular Cages at Molecule−Materials Interfaces. The design and synthesis of cage-forming porphyrin caps and their assembly onto metal surfaces are depicted in Figure 1 and Scheme 1. We reasoned that *α,α,α,α*-atropisomers inspired by the classic picket-fence porphyrin model for hemoglobin oxygen transport[39] would provide a rigid platform to promote a face-to-face arrangement between the porphyrin molecule and metal surface, where thiol-terminated legs built off of the porphyrin scaffold at the ortho positions of the 5,10,15,20 aryl groups serve as multidentate connecting points to bind to the copper electrode material. Self-assembly at the molecular−materials interface would form a cage in which the porphyrin sits like a molecular table on top of the metal surface floor (Figure 1). Accordingly, systematic variation of linkers and metals in both the molecular and materials components of this supramolecular assembly provides an opportunity to explore and optimize catalytic structures and properties. This hybrid approach, where interfacial supramolecular architectures are derived from both molecular and materials building blocks, is complementary to discrete molecular organic cages[40−44] as well as extended porous materials bearing catalytic porphyrin units.[23,45−50]

A general route to the syntheses of *α,α,α,α*-porphyrins and their metalated derivatives is shown in Scheme 1A. Scheme 1B depicts the molecular structures and nomenclatures of the synthesized (metallo)porphyrins along with two porphyrin analogues employed as controls.[51,52] In particular, we synthesized an isostructural *α,α,α,α*-porphyrin with legs that lack terminal thiol pendants for surface binding, as well as a para-substituted tetrathiol porphyrin congener designed to favor edge-on rather than face-to-face interactions with the metal surface. Full synthetic details are given in the Supporting Information.

To generate hybrid supramolecular cages at the molecular−materials interface, metallic copper surfaces were treated with thiol porphyrins generated from in situ deprotection of thioacetate counterparts (Figure 2a).[53] Well-defined metallic Cu films prepared by e-beam evaporation were utilized as model substrates for surface characterization.[54] The successful attachment of the porphyrins to the Cu surface was first evidenced by high-resolution N 1s and S 2p X-ray photoelectron spectroscopy (XPS). The N 1s peak is consistent with a previously reported spectrum assigned to a porphyrin monolayer, confirming the existence of porphyrins on the surface (Figure 2b).[55,56] The S 2p region exhibits two distinct peaks at around ∼161−164 eV and ∼167−169 eV, corresponding to the thiolate and sulfonate species, respectively (Figure 2c).[54] The presence of thiolate species on the surface corroborates possible porphyrin attachment via formation of Cu−S bonds, whereas the sulfonate peaks might be derived from partial thiolate oxidation after air exposure due to the high oxygen permeability of the void spaces in the porphyrin cages. The functionalized Cu surface also shows a slightly wider Cu 2p peak but with lower signal at ∼933 eV compared to the unfunctionalized Cu control surface (Figure S1), which can be reasoned by the surface-attached porphyrin partially oxidizing the Cu surface via Cu−S bond formation. Complementary external reflection Fourier transform infrared spectroscopy (FTIR) measurements provide addition support for porphyrin attachment (Figure S2).

Two potential limiting configurations for porphyrin coordination to the Cu surface may be envisioned, which are anticipated to lead to disparate catalytic performances. In one possible configuration, the porphyrin coordinates with the Cu surface via Cu−S interactions to form a cage architecture where the porphyrin face is elevated above the surface. Another possibility is for the porphyrin face to lie directly on the Cu

DOI: 10.1021/acscentsci.7b00316
ACS Cent. Sci. 2017, 3, 1032−1040

surface through van der Waals interactions, blocking potential access of reactants to the surface. To investigate these possible binding modes, we employed electrochemical underpotential deposition (UPD) studies, in which the measured monolayer thickness of a metal-deposited guest is highly indicative of the number of surface substrate sites that are electrochemically accessible.[57] Porphyrins that orient face-down and promote direct interactions with the Cu surface would block the electrode and result in fewer Cu sites able to be accessed by UPD. In contrast, porphyrins that orient with legs down and favor coordination through Cu−S bonds to create porous cages would leave more Cu sites accessible to the electrolyte solution, resulting in UPD peak areas that are comparable to control Cu surfaces.

To this end, we probed accessible Cu sites by the UPD of lead (Pb) on Cu surfaces in the presence of chloride anions. The standard Cu surfaces (100 nm Cu on Si) show a pair of underpotential deposition and dissolution peaks in the range of −0.05 V to −0.25 V vs standard hydrogen electrode (SHE) (Figure 2d).[58] Treating the Cu surfaces with H_2PAA porphyrins bearing terminal alkene groups shows voltammograms that exhibit smaller peak areas with retained peak shapes and potentials, likely due to the inability of the alkenes to form stable interactions with the Cu surface and possible porphyrin−Cu stacking behavior, both of which would impede Pb deposition. In contrast, the Cu surfaces functionalized with H_2PC_2SH porphyrins bearing terminal thiol groups exhibit almost identical peak areas to control Cu (Figure 2d), showing that porphyrins interacting in this mode do not restrict access to the Cu electrode. Interestingly, the thiol-porphyrin-functionalized Cu surfaces also exhibit a distinct peak shift to more positive potentials, indicating more facile Pb deposition with this molecular attachment (Figure 2d). Taken together, the data suggest that the local electronic structure of the Cu surface has been altered after porphyrin binding, likely due to the partial oxidation of the surface as a result of the formation of Cu−S bonds. The UPD results also imply a high coverage of the porphyrin molecules on the Cu surface since no UPD current is observed at the potential characteristic for unfunctionalized Cu surfaces. The observations from UPD and XPS studies both support the creation of porphyrin cages on a sterically accessible metallic Cu surface via designed Cu−S interactions.

Electrocatalytic CO Reduction with Hybrid Supramolecular Porphyrin Cages Formed on Copper. With these initial hybrid systems in hand, we evaluated their activity for electrocatalytic CO reduction compared to unfunctionalized Cu foils (Figure 3). To compare catalytic activity and selectivity, with particular interest in C−C coupled products, controlled potential electrolysis (CPE) measurements at various potentials were carried out in CO-saturated 0.1 M KOH (aq). The collected gas-phase products were analyzed by gas chromatography (GC), and the liquid-phase products were quantified by ^{1}H NMR (Figure S3). Three major C2 products derived from C−C bond formation—acetate, ethanol, and ethylene—were detected for all electrodes in the potential range of −0.45 V to −0.65 V vs reversible hydrogen electrode (RHE). The faradaic efficiencies (FEs) and specific current densities for each product are shown for direct comparison (Figure 3). As expected, Cu foil alone exhibits low basal activity, with <15% total FE toward CO reduction at relatively low overpotentials (<−0.6 V vs RHE) (Figures 3a−3d and Figure S4) and an appreciable amount of ethylene as the major

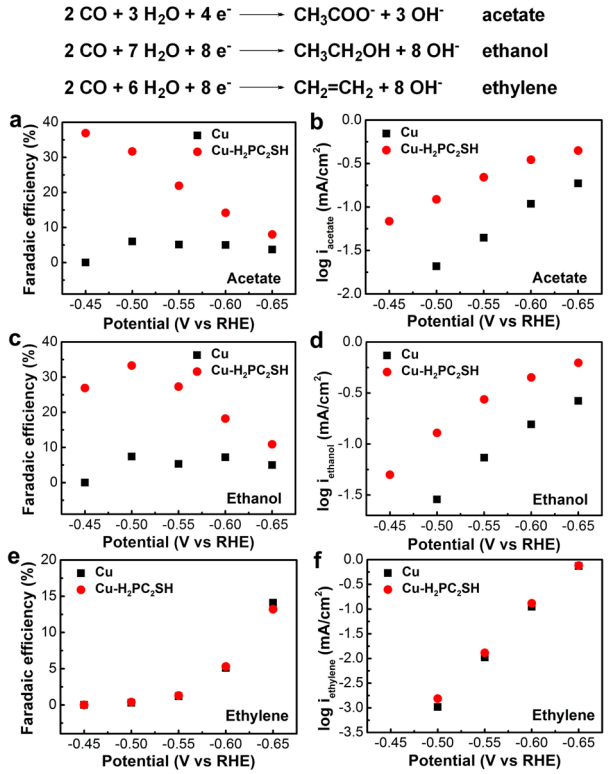

Figure 3. Faradaic efficiencies of CO reduction into (a) acetate, (c) ethanol, and (e) ethylene under different potentials on Cu foil and Cu-H_2PC_2SH in CO-saturated 0.1 M KOH (aq). Specific current densities of CO reduction into (b) acetate, (d) ethanol, and (f) ethylene under different potentials on Cu foil and Cu-H_2PC_2SH in CO-saturated 0.1 M KOH (aq).

product of CO reduction beyond −0.6 V vs RHE, consistent with previous reports (Figures 3e and 3f).[30,33]

We next evaluated the effects of porphyrin functionalization as well as cage size on CO reduction to C−C coupled products by systematically varying the linker lengths in the spacer region (H2PC$_n$SH, n = 1−4). Interestingly, all Cu foils with surface-tethered porphyrins exhibit significantly higher propensities for oxygenate formation (Figure 4). Specifically, an optimal CO reduction selectivity toward oxygenate production was obtained with the two-carbon linker at a potential of −0.55 V vs RHE (Figure 4b). Further expanding the cage size (n = 3, 4) results in a notable decrease in the FEs toward C2 oxygenates. We then compared the activity and selectivity of the optimized Cu-H_2PC_2SH electrode with bare Cu foil under different potentials, and the results show significantly higher FEs and more positive onset potentials for C2 oxygenate formation. More negative applied potentials greatly influence the observed FEs, resulting in reduced amounts of acetate and ethanol production while boosting undesired competitive hydrogen evolution. In contrast, almost identical FEs and current densities were observed on Cu foil and Cu-H_2PC_2SH electrodes for the production of ethylene (Figures 3e and 3f), suggesting that the surface-tethered porphyrin cages affect the reduction pathways toward C2 oxygenate products but not the reduction pathway to this C2 hydrocarbon.

To further probe the nature of the observed enhancements in CO selectivity enabled by supramolecular formation of porphyrin cages on Cu surfaces, we designed a series of control molecules to investigate the roles of these surface-

DOI: 10.1021/acscentsci.7b00316
ACS Cent. Sci. 2017, 3, 1032−1040

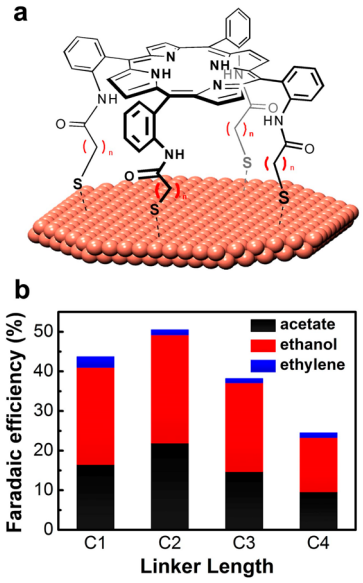

Figure 4. (a) Schematic illustration of free-base porphyrins possessing different linker lengths. (b) Faradaic efficiencies for CO reduction on Cu foils functionalized with free-base porphyrins possessing different linker lengths (Cu-H_2PC_nSH). The electrolyses were performed at a constant potential of −0.55 V vs RHE in CO-saturated 0.1 M KOH (aq).

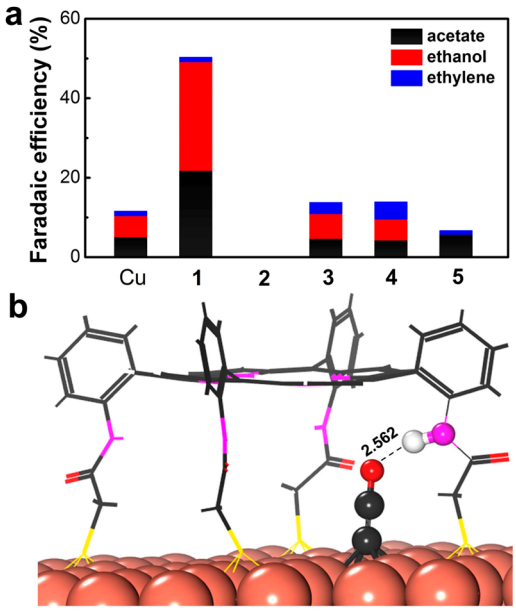

Figure 5. (a) Specific faradaic efficiencies of CO reduction on Cu-H_2PC_2SH in comparison with Cu foil and other control groups. 1: Cu + H_2PC_2SH. 2: Cu + $C_{12}SH$. 3: Cu + 3-MMPA. 4: Cu + H_2PAA. 5: Cu + H_2-*p*-PC_2SH. The electrolysis was performed at a constant potential of −0.55 V vs RHE in CO-saturated 0.1 M KOH (aq). (b) DFT calculation of a speculative ketene intermediate within the porphyrin cage formed on Cu(100) surfaces, which identifies a potential rationalization for differences in CO reduction selectivity for different cage sizes but does not rule out other plausible mechanistic possibilities.

tethered porphyrin caps. Cu surfaces functionalized with simple monothiol additives such as 1-dodecanethiol ($C_{12}SH$), which support conventional self-assembled monolayers (SAMs),[54] or with 3-mercapto-*N*-phenylpropanamide (3-MPPA), which mimics a single linker arm in H_2PC_2SH porphyrins with a pendant amide, were first utilized as thiolate analogues for comparison. The Cu-$C_{12}SH$ electrode exhibits dramatically lowered current densities compared to Cu-H_2PC_2SH, with hydrogen (H_2) as the only major product generated at a potential of −0.55 V vs RHE (Figure 5a and Figure S5). We speculate that this low activity for CO reduction is likely the result of the large energy barrier for diffusing polar CO molecules into the densely packed nonpolar SAMs. Along the same lines, Cu-3-MPPA exhibits lower overall current densities compared to Cu-tethered thiolporphyrins and a characteristic CPE curve with an initial drop followed by a gradual recovery in current density similar to Cu-H_2PC_2SH electrode (Figure 5a and Figure S5). However, the selectivity for this MPPA system toward CO reduction is low, reaching only a ∼10% total FE for carbon products (Figure 3a). Moreover, the para-functionalized porphyrin analogue (Cu-H_2-*p*-PC_2SH) also exhibits significantly lower selectivity toward CO reduction compared to the table-like ortho analogue Cu-H_2-*o*-PC_2SH (Figure 5a). We speculate that the para porphyrins having a flat architecture would either pack by standing edge-on the Cu surfaces via one or two thiolate linkages or lie flat on the surface with direct face-to-face stacking; in either case, these porphyrins are incapable of forming catalytic cages and serve to block accessible Cu sites, thereby lowering electrocatalytic activity and CO selectivity. Finally, the Cu-H_2PAA system bearing terminal alkenes that do not strongly bind copper, mentioned above for UPD studies, exhibits a similar product distribution to bare Cu surfaces (Figure 5a) and reduced surface access as measured by UPD (Figure 2d).

The foregoing results establish that the supramolecular cavity created by the rigid table-like porphyrin scaffold plays a central role in enhancing the selectivity for electrochemical CO reduction to value-added C2 products and over competing water reduction, whereas traditional architectures for molecular functionalization of surfaces through metal−thiol interactions are not beneficial due to the lack of accessible sites on the Cu electrodes. Density functional theory (DFT) calculations on a Cu(100) surface point to a tentative mechanistic proposal involving a ketene intermediate,[59,60] which we speculate may be tuned through hydrogen-bond interactions with the porphyrin cap (Figure 5b and Table S1). Such interactions could rationalize the observed differences in selectivity for CO reduction observed for varying cage sizes but do not rule out other plausible mechanistic possibilities, and further studies must be pursued to address this open question.

The stability of the porphyrin cages on the Cu surfaces was further investigated by UPD and XPS studies (Figure S6). Cu-H_2PC_2SH electrode shows a consistent positive shift of the UPD peak by ∼14 mV compared to the unfunctionalized control Cu electrode. This positive shift is retained after electrolysis, suggesting the persistence of the porphyrin cages on Cu surfaces under CO electroreduction conditions (Figure S6a,b). XPS measurements reveal slight decreases of N 1s and S 2p XPS signals and an increase of Cu 2p XPS signal after electrolysis, indicating some loss of weakly bound porphyrin cages during electrocatalysis (Figure S6c−e), but the retained N 1s and S 2p peaks still suggest the relatively high stability of the porphyrin cages for CO reduction.

Heterobimetallic Supramolecular Porphyrin Cages for Improved CO Reduction Reactivity. In addition to enforcing a rigid cage to maintain surface accessibility as well as orient hydrogen-bond pendants to influence reaction

DOI: 10.1021/acscentsci.7b00316
ACS Cent. Sci. 2017, 3, 1032−1040

selectivity, the porphyrin caps also enable facile introduction and tuning of a second metal site in proximity to the metal electrode center. We anticipated that a second type of metal center has the potential not only to participate as a catalytically active site but also to contribute as a synergistic cofactor to increase local CO concentrations and/or tune the electronic structure of the metal surface for improved CO reduction activity. Indeed, metalloporphyrins have been explored widely in homogeneous catalysis.[14,19,24,61−64] To this end, we screened a series of metals inserted into the two-carbon-linker porphyrin caps (e.g., Fe, Ni, Zn) and observed that the introduction of Fe centers in the porphyrins increases the preference for ethanol production while decreasing the relative ratio of acetate at all potentials applied (Figure 6a,b and Figure S7). An optimal

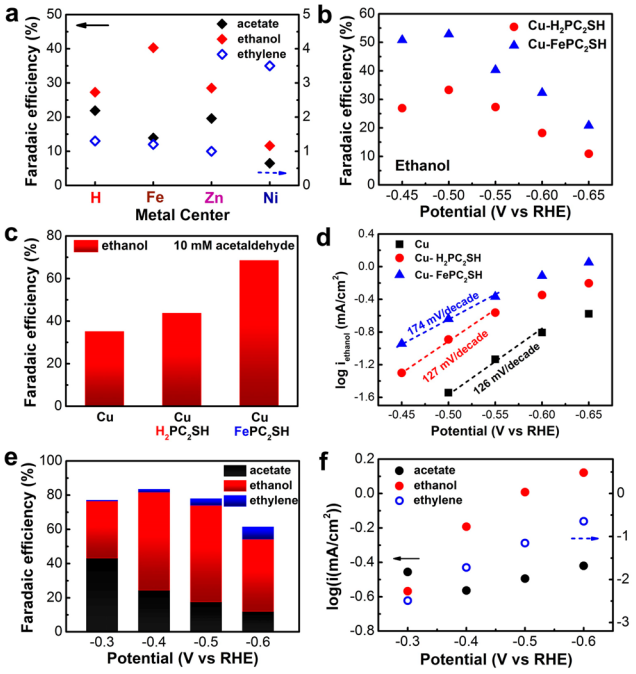

Figure 6. (a) Faradaic efficiencies for CO reduction on Cu foils functionalized with metalloporphyrins containing different metal centers (Cu-MPC$_2$SH). The electrolysis was performed at a constant potential of −0.55 V vs RHE in CO-saturated 0.1 M KOH (aq). (b) Faradaic efficiencies for CO reduction into ethanol under different potentials with Cu-H$_2$PC$_2$SH and Cu-FePC$_2$SH in CO-saturated 0.1 M KOH (aq). (c) Faradaic efficiencies of acetaldehyde reduction into ethanol on Cu foil, Cu-H$_2$PC$_2$SH, and Cu-FePC$_2$SH in Ar-saturated 0.1 M KOH (aq) with 10 mM acetaldehyde at a constant potential of −0.40 V vs RHE. (d) Tafel plots of specific current densities of CO reduction into ethanol on Cu, Cu-H$_2$PC$_2$SH, and Cu-FePC$_2$SH in CO-saturated 0.1 M KOH (aq). (e) Specific faradaic efficiencies and (f) specific current densities of CO reduction on electrodeposited Cu functionalized with iron porphyrins (FePC$_2$SH). The ethylene current density corresponds to the right *y*-axis.

ethanol FE of ∼52% is obtained on a Cu-FePC$_2$SH electrode at a potential of −0.50 V vs RHE (Figure 6b) with good long-term stability over continuous CO reduction electrocatalysis (Figure S8), only losing ca. 10% FE for C2 products over a 24 h period. As expected, functionalization with the redox-inert Zn porphyrin shows comparable product selectivity to that of free-base porphyrins. In contrast, insertion of Ni into porphyrin cap shifts product distributions toward hydrogen formation and a higher FE for ethylene, which may likely be due to the high intrinsic hydrogenation capability of the Ni porphyrins (Figure 6a).[65,66]

With the observation of varying product distributions with different metal substitutions into the porphyrin cap, we next sought to probe aspects of how the Fe derivative promotes higher levels of ethanol production. In this context, previous studies have identified acetaldehyde as a key intermediate for electrochemical CO reduction into ethanol in alkaline media.[67] We thus utilized acetaldehyde as a model substrate for studying the role of Fe in this catalytic process. To this end, the electrocatalytic reductions of acetaldehyde on bare Cu foil, Cu-H$_2$PC$_2$SH, and Cu-FePC$_2$SH electrodes were examined in 0.1 M KOH (aq) with the addition of 10 mM acetaldehyde under Ar atmosphere. The Cu-FePC$_2$SH electrode shows slightly higher activity toward acetaldehyde reduction, with a positive shift in the polarization curves (Figure S9) and much higher FEs toward ethanol production than bare Cu surfaces or Cu functionalized with free-base porphyrin caps (Figure 6c). In fact, Fe porphyrins alone deposited on glassy carbon electrodes show moderate activity toward acetaldehyde reduction with a reasonable current density within the potential range for CO reduction (Figure S9), which is consistent with previous findings that Fe porphyrins can be effectively used as catalysts for the hydrogenation of various aldehydes and ketones.[68] As such, we propose that Fe porphyrins might participate in reduction of acetaldehyde intermediates, which in turn favors increased ethanol production in electrochemical CO reduction. Indeed, the Tafel plot of the specific ethanol current densities on Cu-FePC$_2$SH electrodes shows a much earlier onset potential but exhibits a larger Tafel slope of 174 mV/dec (Figure 6d). This deviation from the Tafel slopes of 126 and 127 mV/dec observed on Cu foil and on Cu-H$_2$PC$_2$SH electrodes, respectively, supports the participation of Fe porphyrins in the rate-determining step of the ethanol production pathway, with observation of a larger Tafel slope for the Fe−Cu bimetallic system compared to Cu-only congeners resulting from inefficiencies in charge transfer between the Fe porphyrin and Cu surface. Evidence for this notion is provided by the larger charge transfer resistance under CO atmosphere compared to Ar (Figure S10), and future efforts will aim to increase charge transfer efficiency.

Finally, we sought to optimize the CO reduction activity of these hybrid heterobimetallic systems, using the Cu-FePC$_2$SH porphyrin catalyst showing the best product selectivity toward the liquid fuel ethanol as a starting point. Previous work highlights the significance of exposed Cu facets for electrochemical CO$_2$ or CO reductions,[26,60,69−74] where Cu(100) or other high-energy facets are more active than the thermodynamically more stable Cu(111) surfaces and can enhance formation of CO dimerized products.[26,60,71,73,75,76] We employed electrodeposition of Cu on glassy carbon in chloride-containing aqueous CuSO$_4$ electrolyte as a general and facile way of controlling the exposed facets of the Cu substrates.[77,78] The supramolecular catalyst systems formed by combination of the FePC$_2$SH porphyrin caps with electrodeposited Cu exhibit markedly higher specific current densities at low overpotentials (Figure 6f). The CO reduction product distribution is relatively similar to that of Fe porphyrin cages on Cu foils, but with slightly lower FEs for hydrogen production (Figure 6e). The higher current densities allow for quantitative analyses of the products at even lower overpotentials where competitive hydrogen evolution is insignificant. Specifically, at −0.4 V vs RHE, the catalyst achieves a total FE of 83% toward

DOI: 10.1021/acscentsci.7b00316
ACS Cent. Sci. 2017, 3, 1032−1040

CO reduction into C2 products, with 57% FE for ethanol and 24% FE for acetate at a current density of 1.34 mA/cm^2 (Figure 6e).

CONCLUSIONS

In summary, we have presented a supramolecular strategy for electrocatalytic carbon fixation to multicarbon products through the self-assembly of synthetic cages at molecular−materials interfaces. Porphyrin capping units with directional legs terminated by thiol ligands form face-to-face cavities upon binding copper electrodes that leave surface sites electrochemically accessible. Varying linker lengths as well as metal substitutions in the porphyrin core provide versatile molecular handles for tuning selectivity and activity for electrochemical CO reduction to carbon−carbon coupled products. The heterobimetallic molecular materials formed by assembly of the C2-linked Fe porphyrin derivative on Cu achieve up to 83% FE for CO reduction into C2 products, with up to 57% ethanol and 24% acetate generated at −0.4 V vs RHE and a current density of 1.34 mA/cm^2. These values represent an order of magnitude improvement over unfunctionalized copper electrodes. Further experiments suggest that the Fe center can aid in cooperative reduction of potential acetaldehyde intermediates. Moreover, control analogues that lack thiol binding groups as well as positional isomers favoring edge-on binding or direct van der Waals stacking exhibit reduced surface access and negligible CO over water reduction selectivity, pointing to a critical role for the three-dimensional pocket in catalysis. In addition to establishing a unique electrochemical platform for reducing CO to value-added C2 oxygenates, this work provides a starting point for the design of supramolecular architectures at molecular−materials interfaces for a broader range of chemical transformations and applications of interest.

ASSOCIATED CONTENT

Supporting Information

The Supporting Information is available free of charge on the ACS Publications website at DOI: 10.1021/acscentsci.7b00316.

Experimental details and data (PDF)

AUTHOR INFORMATION

Corresponding Author

*E-mail: chrischang@berkeley.edu.

ORCID

Xiaodong Wen: 0000-0001-5626-8581

Christopher J. Chang: 0000-0001-5732-9497

Author Contributions

§M.G., Z.C., and W.L. contributed equally to this work.

Notes

The authors declare no competing financial interest.

ACKNOWLEDGMENTS

Financial support for synthesis, characterization, calculations, and electrochemical measurements was provided by DOE/LBNL Grant 101528-002 (C.J.C.). C.J.C. is an Investigator with the Howard Hughes Medical Institute and a CIFAR Senior Fellow. E.M.N. and P.T.S. acknowledge support from the NSF Graduate Research Fellowship Program. We also thank Jun Xu for advice and support on NMR experiments, Chang Yan for help on the external reflection FTIR studies, and Dr. Jayeon Baek for help on the XPS studies.

REFERENCES

(1) Lewis, N. S.; Nocera, D. G. Powering the planet: Chemical challenges in solar energy utilization. *Proc. Natl. Acad. Sci. U. S. A.* **2006**, *103* (43), 15729.

(2) Gray, H. B. Powering the planet with solar fuel. *Nat. Chem.* **2009**, *1* (1), 7.

(3) Kumar, B.; Llorente, M.; Froehlich, J.; Dang, T.; Sathrum, A.; Kubiak, C. P. Photochemical and photoelectrochemical reduction of CO2. *Annu. Rev. Phys. Chem.* **2012**, *63*, 541.

(4) Appel, A. M.; Bercaw, J. E.; Bocarsly, A. B.; Dobbek, H.; DuBois, D. L.; Dupuis, M.; Ferry, J. G.; Fujita, E.; Hille, R.; Kenis, P. J. A.; Kerfeld, C. A.; Morris, R. H.; Peden, C. H. F.; Portis, A. R.; Ragsdale, S. W.; Rauchfuss, T. B.; Reek, J. N. H.; Seefeldt, L. C.; Thauer, R. K.; Waldrop, G. L. Frontiers, Opportunities, and Challenges in Biochemical and Chemical Catalysis of CO2 Fixation. *Chem. Rev.* **2013**, *113* (8), 6621.

(5) Costentin, C.; Robert, M.; Savéant, J.-M. Catalysis of the electrochemical reduction of carbon dioxide. *Chem. Soc. Rev.* **2013**, *42* (6), 2423.

(6) Elgrishi, N.; Chambers, M. B.; Wang, X.; Fontecave, M. Molecular polypyridine-based metal complexes as catalysts for the reduction of CO 2. *Chem. Soc. Rev.* **2017**, *46* (3), 761.

(7) Liu, M.; Pang, Y. J.; Zhang, B.; De Luna, P.; Voznyy, O.; Xu, J. X.; Zheng, X. L.; Dinh, C. T.; Fan, F. J.; Cao, C. H.; de Arquer, F. P. G.; Safaei, T. S.; Mepham, A.; Klinkova, A.; Kumacheva, E.; Filleter, T.; Sinton, D.; Kelley, S. O.; Sargent, E. H. Enhanced electrocatalytic CO_2 reduction via field-induced reagent concentration. *Nature* **2016**, *537* (7620), 382.

(8) Fisher, B. J.; Eisenberg, R. Electrocatalytic reduction of carbon dioxide by using macrocycles of nickel and cobalt. *J. Am. Chem. Soc.* **1980**, *102* (24), 7361.

(9) Hawecker, J.; Lehn, J.-M.; Ziessel, R. Electrocatalytic reduction of carbon dioxide mediated by Re (bipy)(CO) 3 Cl (bipy= 2, 2′-bipyridine). *J. Chem. Soc., Chem. Commun.* **1984**, No. 6, 328.

(10) Hori, Y.; Kikuchi, K.; Suzuki, S. Production of CO and CH4 in electrochemical reduction of CO2 at metal electrodes in aqueous hydrogencarbonate solution. *Chem. Lett.* **1985**, *14* (11), 1695.

(11) Beley, M.; Collin, J. P.; Ruppert, R.; Sauvage, J. P. Electrocatalytic reduction of carbon dioxide by nickel cyclam2+ in water: study of the factors affecting the efficiency and the selectivity of the process. *J. Am. Chem. Soc.* **1986**, *108* (24), 7461.

(12) Rosen, B. A.; Salehi-Khojin, A.; Thorson, M. R.; Zhu, W.; Whipple, D. T.; Kenis, P. J.; Masel, R. I. Ionic liquid−mediated selective conversion of CO2 to CO at low overpotentials. *Science* **2011**, *334* (6056), 643.

(13) Thoi, V. S.; Chang, C. J. Nickel N-heterocyclic carbene−pyridine complexes that exhibit selectivity for electrocatalytic reduction of carbon dioxide over water. *Chem. Commun.* **2011**, *47* (23), 6578.

(14) Costentin, C.; Drouet, S.; Robert, M.; Savéant, J.-M. A local proton source enhances CO2 electroreduction to CO by a molecular Fe catalyst. *Science* **2012**, *338* (6103), 90.

(15) Schneider, J.; Jia, H.; Kobiro, K.; Cabelli, D. E.; Muckerman, J. T.; Fujita, E. Nickel (II) macrocycles: highly efficient electrocatalysts for the selective reduction of CO 2 to CO. *Energy Environ. Sci.* **2012**, *5* (11), 9502.

(16) Smieja, J. M.; Sampson, M. D.; Grice, K. A.; Benson, E. E.; Froehlich, J. D.; Kubiak, C. P. Manganese as a substitute for rhenium in CO2 reduction catalysts: The importance of acids. *Inorg. Chem.* **2013**, *52* (5), 2484.

(17) Thoi, V. S.; Kornienko, N.; Margarit, C. G.; Yang, P.; Chang, C. J. Visible-Light Photoredox Catalysis: Selective Reduction of Carbon Dioxide to Carbon Monoxide by a Nickel N-Heterocyclic Carbene−Isoquinoline Complex. *J. Am. Chem. Soc.* **2013**, *135* (38), 14413.

(18) Zhu, W.; Michalsky, R.; Metin, Ö.; Lv, H.; Guo, S.; Wright, C. J.; Sun, X.; Peterson, A. A.; Sun, S. Monodisperse Au nanoparticles for selective electrocatalytic reduction of CO2 to CO. *J. Am. Chem. Soc.* **2013**, *135* (45), 16833.

(19) Costentin, C.; Passard, G.; Robert, M.; Savéant, J.-M. Ultraefficient homogeneous catalyst for the CO2-to-CO electro-

DOI: 10.1021/acscentsci.7b00316
ACS Cent. Sci. 2017, 3, 1032−1040

chemical conversion. *Proc. Natl. Acad. Sci. U. S. A.* **2014**, *111* (42), 14990.
(20) Kim, D.; Resasco, J.; Yu, Y.; Asiri, A. M.; Yang, P. Synergistic geometric and electronic effects for electrochemical reduction of carbon dioxide using gold−copper bimetallic nanoparticles. *Nat. Commun.* **2014**, *5*, 4948.
(21) Zhu, W.; Zhang, Y.-J.; Zhang, H.; Lv, H.; Li, Q.; Michalsky, R.; Peterson, A. A.; Sun, S. Active and selective conversion of CO2 to CO on ultrathin Au nanowires. *J. Am. Chem. Soc.* **2014**, *136* (46), 16132.
(22) Hall, A. S.; Yoon, Y.; Wuttig, A.; Surendranath, Y. Mesostructure-induced selectivity in CO2 reduction catalysis. *J. Am. Chem. Soc.* **2015**, *137* (47), 14834.
(23) Lin, S.; Diercks, C. S.; Zhang, Y. B.; Kornienko, N.; Nichols, E. M.; Zhao, Y. B.; Paris, A. R.; Kim, D.; Yang, P.; Yaghi, O. M.; Chang, C. J. Covalent organic frameworks comprising cobalt porphyrins for catalytic CO2 reduction in water. *Science* **2015**, *349* (6253), 1208.
(24) Azcarate, I.; Costentin, C.; Robert, M.; Savéant, J.-M. Through-Space Charge Interaction Substituent Effects in Molecular Catalysis Leading to the Design of the Most Efficient Catalyst of CO2-to-CO Electrochemical Conversion. *J. Am. Chem. Soc.* **2016**, *138* (51), 16639.
(25) Cao, Z.; Kim, D.; Hong, D. C.; Yu, Y.; Xu, J.; Lin, S.; Wen, X. D.; Nichols, E. M.; Jeong, K.; Reimer, J. A.; Yang, P. D.; Chang, C. J. A Molecular Surface Functionalization Approach to Tuning Nanoparticle Electrocatalysts for Carbon Dioxide Reduction. *J. Am. Chem. Soc.* **2016**, *138* (26), 8120.
(26) Wang, Z.; Yang, G.; Zhang, Z.; Jin, M.; Yin, Y. Selectivity on Etching: Creation of High-Energy Facets on Copper Nanocrystals for CO2 Electrochemical Reduction. *ACS Nano* **2016**, *10* (4), 4559.
(27) Hong, D.; Tsukakoshi, Y.; Kotani, H.; Ishizuka, T.; Kojima, T. Visible-Light-Driven Photocatalytic CO_2 Reduction by a Ni (II) Complex Bearing a Bioinspired Tetradentate Ligand for Selective CO Production. *J. Am. Chem. Soc.* **2017**, *139* (19), 6538.
(28) Iglesia, E. Design, synthesis, and use of cobalt-based Fischer−Tropsch synthesis catalysts. *Appl. Catal., A* **1997**, *161* (1−2), 59.
(29) Khodakov, A. Y.; Chu, W.; Fongarland, P. Advances in the development of novel cobalt Fischer− Tropsch catalysts for synthesis of long-chain hydrocarbons and clean fuels. *Chem. Rev.* **2007**, *107* (5), 1692.
(30) Li, C. W.; Ciston, J.; Kanan, M. W. Electroreduction of carbon monoxide to liquid fuel on oxide-derived nanocrystalline copper. *Nature* **2014**, *508* (7497), 504.
(31) Verdaguer-Casadevall, A.; Li, C. W.; Johansson, T. P.; Scott, S. B.; McKeown, J. T.; Kumar, M.; Stephens, I. E.; Kanan, M. W.; Chorkendorff, I. Probing the active surface sites for CO reduction on oxide-derived copper electrocatalysts. *J. Am. Chem. Soc.* **2015**, *137* (31), 9808.
(32) Feng, X.; Jiang, K.; Fan, S.; Kanan, M. W. A direct grain-boundary-activity correlation for CO electroreduction on Cu nanoparticles. *ACS Cent. Sci.* **2016**, *2* (3), 169.
(33) Hori, Y.; Murata, A.; Takahashi, R.; Suzuki, S. Electroreduction of carbon monoxide to methane and ethylene at a copper electrode in aqueous solutions at ambient temperature and pressure. *J. Am. Chem. Soc.* **1987**, *109* (16), 5022.
(34) Drennan, C. L.; Heo, J.; Sintchak, M. D.; Schreiter, E.; Ludden, P. W. Life on carbon monoxide: X-ray structure of Rhodospirillum rubrum Ni-Fe-S carbon monoxide dehydrogenase. *Proc. Natl. Acad. Sci. U. S. A.* **2001**, *98* (21), 11973.
(35) Dobbek, H.; Gremer, L.; Kiefersauer, R.; Huber, R.; Meyer, O. Catalysis at a dinuclear [CuSMo (O) OH] cluster in a CO dehydrogenase resolved at 1.1-Å resolution. *Proc. Natl. Acad. Sci. U. S. A.* **2002**, *99* (25), 15971.
(36) Reda, T.; Plugge, C. M.; Abram, N. J.; Hirst, J. Reversible interconversion of carbon dioxide and formate by an electroactive enzyme. *Proc. Natl. Acad. Sci. U. S. A.* **2008**, *105* (31), 10654.
(37) Cracknell, J. A.; Vincent, K. A.; Armstrong, F. A. Enzymes as working or inspirational electrocatalysts for fuel cells and electrolysis. *Chem. Rev.* **2008**, *108* (7), 2439.
(38) Woolerton, T. W.; Sheard, S.; Reisner, E.; Pierce, E.; Ragsdale, S. W.; Armstrong, F. A. Efficient and clean photoreduction of CO2 to CO by enzyme-modified TiO2 nanoparticles using visible light. *J. Am. Chem. Soc.* **2010**, *132* (7), 2132.
(39) Collman, J. P.; Zhang, X.; Wong, K.; Brauman, J. I. Dioxygen binding in iron and cobalt picnic basket porphyrins. *J. Am. Chem. Soc.* **1994**, *116* (14), 6245.
(40) Anderson, H. L.; Sanders, J. K. Synthesis of a cyclic porphyrin trimer with a semi-rigid cavity. *J. Chem. Soc., Chem. Commun.* **1989**, *22*, 1714.
(41) Anderson, H. L.; Sanders, J. K. Amine-Template-Directed Synthesis of Cyclic Porphyrin Oligomers. *Angew. Chem., Int. Ed. Engl.* **1990**, *29* (12), 1400.
(42) Hong, S.; Rohman, M.; Jia, J.; Kim, Y.; Moon, D.; Kim, Y.; Ko, Y. H.; Lee, E.; Kim, K. Porphyrin boxes: rationally designed porous organic cages. *Angew. Chem., Int. Ed.* **2015**, *54* (45), 13241.
(43) Benke, B. P.; Aich, P.; Kim, Y.; Kim, K. L.; Rohman, M. R.; Hong, S.; Hwang, I.-C.; Lee, E. H.; Roh, J. H.; Kim, K. Iodide-Selective Synthetic Ion Channels Based on Shape-persistent Organic Cages. *J. Am. Chem. Soc.* **2017**, *139* (22), 7432.
(44) Cooper, A. I. Porous Molecular Solids and Liquids. *ACS Cent. Sci.* **2017**, *3* (6), 544.
(45) Shultz, A. M.; Farha, O. K.; Hupp, J. T.; Nguyen, S. T. A catalytically active, permanently microporous MOF with metal-loporphyrin struts. *J. Am. Chem. Soc.* **2009**, *131* (12), 4204.
(46) Lee, C. Y.; Farha, O. K.; Hong, B. J.; Sarjeant, A. A.; Nguyen, S. T.; Hupp, J. T. Light-harvesting metal−organic frameworks (MOFs): efficient strut-to-strut energy transfer in bodipy and porphyrin-based MOFs. *J. Am. Chem. Soc.* **2011**, *133* (40), 15858.
(47) Hod, I.; Sampson, M. D.; Deria, P.; Kubiak, C. P.; Farha, O. K.; Hupp, J. T. Fe-porphyrin-based metal−organic framework films as high-surface concentration, heterogeneous catalysts for electrochemical reduction of CO2. *ACS Catal.* **2015**, *5* (11), 6302.
(48) Kornienko, N.; Zhao, Y.; Kley, C. S.; Zhu, C.; Kim, D.; Lin, S.; Chang, C. J.; Yaghi, O. M.; Yang, P. Metal−organic frameworks for electrocatalytic reduction of carbon dioxide. *J. Am. Chem. Soc.* **2015**, *137* (44), 14129.
(49) Wan, S.; Gandara, F.; Asano, A.; Furukawa, H.; Saeki, A.; Dey, S. K.; Liao, L.; Ambrogio, M. W.; Botros, Y. Y.; Duan, X. F.; Seki, S.; Stoddart, J. F.; Yaghi, O. M. Covalent Organic Frameworks with High Charge Carrier Mobility. *Chem. Mater.* **2011**, *23* (18), 4094.
(50) Smith, B. J.; Parent, L. R.; Overholts, A. C.; Beaucage, P. A.; Bisbey, R. P.; Chavez, A. D.; Hwang, N.; Park, C.; Evans, A. M.; Gianneschi, N. C.; Dichtel, W. R. Colloidal Covalent Organic Frameworks. *ACS Cent. Sci.* **2017**, *3* (1), 58.
(51) Ohyama, J.; Hitomi, Y.; Higuchi, Y.; Tanaka, T. Size controlled synthesis of gold nanoparticles by porphyrin with four sulfur atoms. *Top. Catal.* **2009**, *52* (6−7), 852.
(52) Hitomi, Y.; Aoki, K.; Miyachi, R.; Ohyama, J.; Kodera, M.; Tanaka, T.; Sugihara, F. Gold Nanoparticles Coated with Manganese−Porphyrin That Effectively Shorten the Longitudinal Relaxation Time of Water Molecules Depending on the Particle Size. *Chem. Lett.* **2014**, *43* (12), 1901.
(53) Pakiari, A.; Jamshidi, Z. Nature and strength of M− S Bonds (M= Au, Ag, and Cu) in binary alloy gold clusters. *J. Phys. Chem. A* **2010**, *114* (34), 9212.
(54) Laibinis, P. E.; Whitesides, G. M. Self-assembled monolayers of n-alkanethiolates on copper are barrier films that protect the metal against oxidation by air. *J. Am. Chem. Soc.* **1992**, *114* (23), 9022.
(55) Gassman, P. G.; Ghosh, A.; Almlof, J. Electronic effects of peripheral substituents in porphyrins: x-ray photoelectron spectroscopy and ab initio self-consistent field calculations. *J. Am. Chem. Soc.* **1992**, *114* (25), 9990.
(56) Lal, C.; Caputo, M.; Goldoni, A.; Jain, I. Conformational adaptation of 2H-Tetraphenylporphyrin at Fe/Si (100) interface during metalation. *J. Mater. Res. Technol.* **2014**, *3* (1), 42.
(57) Herrero, E.; Buller, L. J.; Abruña, H. D. Underpotential deposition at single crystal surfaces of Au, Pt, Ag and other materials. *Chem. Rev.* **2001**, *101* (7), 1897.
(58) Brisard, G. M.; Zenati, E.; Gasteiger, H. A.; Markovic, N.; Ross, P. N., Jr Underpotential deposition of lead on Copper (111): A study

DOI: 10.1021/acscentsci.7b00316
ACS Cent. Sci. 2017, 3, 1032−1040

using a single-crystal rotating ring disk electrode and ex situ low-energy electron diffraction and scanning tunneling microscopy. *Langmuir* **1995**, *11* (6), 2221.
(59) Xiao, H.; Cheng, T.; Goddard, W. A. Atomistic Mechanisms Underlying Selectivities in C1 and C2 Products from Electrochemical Reduction of CO on Cu (111). *J. Am. Chem. Soc.* **2017**, *139* (1), 130.
(60) Cheng, T.; Xiao, H.; Goddard, W. A. Full atomistic reaction mechanism with kinetics for CO reduction on Cu (100) from ab initio molecular dynamics free-energy calculations at 298 K. *Proc. Natl. Acad. Sci. U. S. A.* **2017**, *114* (8), 1795.
(61) Kellett, R. M.; Spiro, T. G. Cobalt (I) porphyrin catalysts of hydrogen production from water. *Inorg. Chem.* **1985**, *24* (15), 2373.
(62) Liu, W.; Huang, X.; Cheng, M.-J.; Nielsen, R. J.; Goddard, W. A.; Groves, J. T. Oxidative aliphatic CH fluorination with fluoride ion catalyzed by a manganese porphyrin. *Science* **2012**, *337* (6100), 1322.
(63) Kleingardner, J. G.; Kandemir, B.; Bren, K. L. Hydrogen evolution from neutral water under aerobic conditions catalyzed by cobalt microperoxidase-11. *J. Am. Chem. Soc.* **2014**, *136* (1), 4.
(64) McLaughlin, M. P.; Retegan, M.; Bill, E.; Payne, T. M.; Shafaat, H. S.; Pena, S.; Sudhamsu, J.; Ensign, A. A.; Crane, B. R.; Neese, F.; Holland, P. L. Azurin as a Protein Scaffold for a Low-coordinate Nonheme Iron Site with a Small-molecule Binding Pocket. *J. Am. Chem. Soc.* **2012**, *134* (48), 19746.
(65) Bediako, D. K.; Solis, B. H.; Dogutan, D. K.; Roubelakis, M. M.; Maher, A. G.; Lee, C. H.; Chambers, M. B.; Hammes-Schiffer, S.; Nocera, D. G. Role of pendant proton relays and proton-coupled electron transfer on the hydrogen evolution reaction by nickel hangman porphyrins. *Proc. Natl. Acad. Sci. U. S. A.* **2014**, *111* (42), 15001.
(66) Han, Y. Z.; Fang, H. Y.; Jing, H. Z.; Sun, H. L.; Lei, H. T.; Lai, W. Z.; Cao, R. Singly versus Doubly Reduced Nickel Porphyrins for Proton Reduction: Experimental and Theoretical Evidence for a Homolytic Hydrogen-Evolution Reaction. *Angew. Chem., Int. Ed.* **2016**, *55* (18), 5457.
(67) Bertheussen, E.; Verdaguer-Casadevall, A.; Ravasio, D.; Montoya, J. H.; Trimarco, D. B.; Roy, C.; Meier, S.; Wendland, J.; Norskov, J. K.; Stephens, I. E. L.; Chorkendorff, I. Acetaldehyde as an Intermediate in the Electroreduction of Carbon Monoxide to Ethanol on Oxide-Derived Copper. *Angew. Chem., Int. Ed.* **2016**, *55* (4), 1450.
(68) Junge, K.; Schröder, K.; Beller, M. Homogeneous catalysis using iron complexes: recent developments in selective reductions. *Chem. Commun.* **2011**, *47* (17), 4849.
(69) Schouten, K.; Kwon, Y.; Van der Ham, C.; Qin, Z.; Koper, M. A new mechanism for the selectivity to C 1 and C 2 species in the electrochemical reduction of carbon dioxide on copper electrodes. *Chem. Sci.* **2011**, *2* (10), 1902.
(70) Roberts, F. S.; Kuhl, K. P.; Nilsson, A. High selectivity for ethylene from carbon dioxide reduction over copper nanocube electrocatalysts. *Angew. Chem., Int. Ed.* **2015**, *54* (17), 5179.
(71) Luo, W.; Nie, X.; Janik, M. J.; Asthagiri, A. Facet Dependence of CO2 Reduction Paths on Cu Electrodes. *ACS Catal.* **2016**, *6* (1), 219.
(72) Loiudice, A.; Lobaccaro, P.; Kamali, E. A.; Thao, T.; Huang, B. H.; Ager, J. W.; Buonsanti, R. Tailoring Copper Nanocrystals towards C2 Products in Electrochemical CO2 Reduction. *Angew. Chem., Int. Ed.* **2016**, *55* (19), 5789.
(73) Pérez-Gallent, E.; Figueiredo, M. C.; Calle-Vallejo, F.; Koper, M. Spectroscopic Observation of a Hydrogenated CO Dimer Intermediate During CO Reduction on Cu (100) Electrodes. *Angew. Chem.* **2017**, *129* (13), 3675.
(74) Li, Y.; Cui, F.; Ross, M. B.; Kim, D.; Sun, Y.; Yang, P. Structure-Sensitive CO2 Electroreduction to Hydrocarbons on Ultrathin 5-fold Twinned Copper Nanowires. *Nano Lett.* **2017**, *17* (2), 1312.
(75) Schouten, K. J. P.; Qin, Z.; Pérez Gallent, E.; Koper, M. T. M. Two pathways for the formation of ethylene in CO reduction on single-crystal copper electrodes. *J. Am. Chem. Soc.* **2012**, *134* (24), 9864.
(76) Kim, Y.-G.; Javier, A.; Baricuatro, J. H.; Torelli, D.; Cummins, K. D.; Tsang, C. F.; Hemminger, J. C.; Soriaga, M. P. Surface reconstruction of pure-Cu single-crystal electrodes under CO-reduction potentials in alkaline solutions: A study by seriatim ECSTM-DEMS. *J. Electroanal. Chem.* **2016**, *780*, 290.
(77) Lakshmanan, V.; Mackinnon, D.; Brannen, J. The effect of chloride ion in the electrowinning of copper. *J. Appl. Electrochem.* **1977**, *7* (1), 81.
(78) Shao, W.; Zangari, G. Dendritic growth and morphology selection in copper electrodeposition from acidic sulfate solutions containing chlorides. *J. Phys. Chem. C* **2009**, *113* (23), 10097.

DOI: 10.1021/acscentsci.7b00316
ACS Cent. Sci. 2017, 3, 1032−1040